OPEN ACCESS

University of BRISTOL

Watanabe, N., & Stoten, D. P. (2016). Actuator control for a rapid prototyping railway bogie, using a dynamically substructured systems approach. *Quarterly Report of RTRI (Railway Technical Research Institute)*, *57*(2), 90-97. https://doi.org/10.2219/rtriqr.57.2_90

Peer reviewed version

Link to published version (if available):
10.2219/rtriqr.57.2_90

Link to publication record in Explore Bristol Research
PDF-document

University of Bristol - Explore Bristol Research

General rights

Actuator Control for a Rapid Prototyping Railway Bogie, using a Dynamically Substructured Systems Approach [1]

Nobuyuki WATANABE, Running Gear Laboratory, Vehicle Structure Technology Division

David P. STOTEN, Advanced Control and Test Laboratory, University of Bristol, UK

A rapid prototyping bogie (RPB) has multiple actuators to emulate missing bogie components. In the original RPB hybrid control system, deterioration in the control performance, which was caused by dynamic coupling between the multiple actuators, was observed during the RPB performance tests. To solve this issue, a new controller was developed, based upon the dynamically substructured systems (DSS) method, and trialled on an existing proof-of-concept test rig. Through random excitation tests, it was confirmed that the actuators were well controlled. As a consequence, the DSS approach was determined as a viable framework for future research into the RPB system.

Key words: *Hybrid Testing, Rapid Prototyping Bogie, Dynamically Substructured Systems, Automatic Control, State-Space Methods, Dynamic Coupling, Railway Vehicle Design*

1. Introduction

Rapid prototyping is a form of advanced testing, the concepts of which are now receiving more interest in product design. In rapid prototyping tests, actuators substitute for missing components and, with suitable control, can emulate their characteristics. This enables the evaluation of product performance under virtually real conditions before manufacturing the final product, not only reducing time and cost by omitting the prototyping stage, but also improving

quality by allowing more time for testing. Using this technique, RTRI has developed a rapid prototyping bogie (RPB) [2]. The RPB has 9 electrical actuators to substitute for missing bogie suspension components, and its purpose is to determine an optimal parameter set for them on the rolling stock test plant (RSTP) at RTRI.

Thus, the original RPB controller was based upon a hybrid testing technique using numerical (virtual suspension) models and physical components (actuators and other bogie components). The technique was deemed suitable for the RPB because it was straightforward to change the characteristics of virtual suspensions simply by replacing them with their numerical models. The actuators were force-controlled independently of each other, according to the behaviour of a virtual suspension device model (i.e. a reference model). Although the controller behaved satisfactorily when each actuator was shaken independently, unexpected high frequency components were observed in the RPB performance tests [3]. It was concluded that dynamic coupling between the multiple actuators caused this deterioration in the control performance of the RPB and that a more effective technique was required.

In more recent years, a new form of mixed physical-numerical strategy has been developed, called the dynamic substructuring system testing method (or DSS, for short), which is an alternative to hybrid testing. Although it is more complicated to design than the hybrid test system, DSS has the significant advantage of ensuring stable and accurate synchronisation of multi-axis numerical and physical substructures at their common boundaries, even in the face of dynamic uncertainty. This new approach was first described in the reference [4], which allowed for linear or adaptive algorithms (or a combination thereof) in the process of controlled synchronisation. A description of this DSS approach applied to the RPB problem therefore forms the core of this paper.

The rest of this paper is structured as follows. An outline of the RPB is presented in section 2, including observed issues in the previous tests. In section 3, implementation tests using the

existing proof-of-concept rig are described. Although components of this rig are different from those of the RPB, a similar single wheel-set model and appropriate parameter sets of the virtual device are used. Therefore the rig tests are fundamentally similar to those used on the RPB. Controlled performance comparisons are conducted via simulations in section 4. Finally, section 5 draws together the main conclusions from this work.

2. Overview of the original RPB scheme at RTRI

2.1 RPB system

The RPB, shown in Fig. 1, has 9 electric actuators: (a) 4 longitudinal actuators for longitudinal axle box stiffness, (b) 2 anti-yawing actuators, (c) 2 vertical actuators for vertical stiffness of the air springs and (d) 1 lateral actuator representing the lateral damping and stiffness of the air springs. Actuators in (a) and (b) substitute directly for the corresponding bogie suspension components, and the others compensate for existing suspensions, such as air springs, for emulating the characteristics of the missing suspensions.
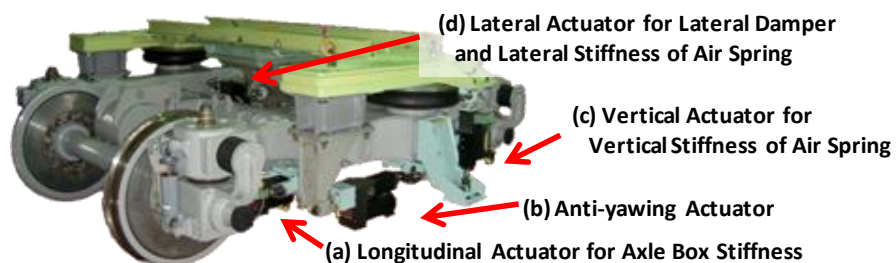

(d) Lateral Actuator for Lateral Damper and Lateral Stiffness of Air Spring

(c) Vertical Actuator for Vertical Stiffness of Air Spring

(b) Anti-yawing Actuator

(a) Longitudinal Actuator for Axle Box Stiffness

Fig. 1 Overview of the RPB

Under normal straight-track conditions, motions of axle boxes in the longitudinal direction, together with the stroke amplitudes of anti-yawing dampers, are less than 1 mm. Their characteristics have a significant effect on bogie stability; therefore any gaps at points of attachment should be avoided. Nevertheless, the RPB actuators require some protection from

excessive bending moments. To cope with these demands, crossed roller bearings and rubber bushes are used at the ends of actuators in (a) and (b), above. Figure 2 shows an anti-yawing actuator with a bending moment protection mechanism. The controller can acquire actuator displacement and force outputs via a servo-motor rotational encoder and load cell, but cannot directly access rubber deformation information, due to the lack of a suitable sensor.
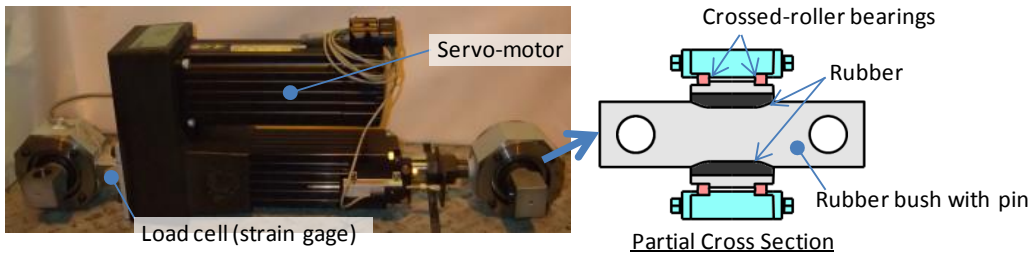

Fig. 2   Overview of anti-yawing actuator

2.2 Hybrid controller

As described above, in the original RTRI scheme the actuators were force-controlled independently of each other using a hybrid scheme, according to the output of the corresponding reference model; see Fig. 3. The external controller was built using Matlab Simulink and xPCTarget. Each fixed feedback gain was determined via independent shaking tests.
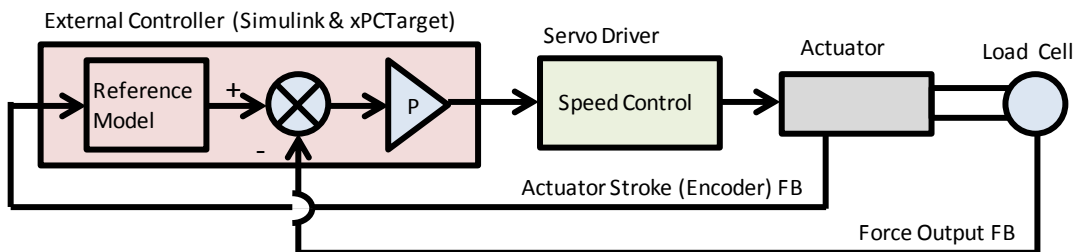

Fig. 3   Hybrid controller diagram for the RPB actuator

2.3 Original RPB tests

Figure 4 shows a single test-bench shaking test result, together with a RSTP performance test result conducted on a longitudinal actuator. The force output tracked the demand with

sufficient accuracy when the actuator was shaken independently. However there were two unexpected peaks in the power spectral density (PSD) curve at 7.7Hz and 14Hz, which were beyond the frequency bandwidth of the roller rig excitation. Note that the running speed of the performance test was 50km/h; therefore the RPB should remain in a stable condition. Consequently, it was concluded that dynamic coupling between the multiple actuators caused this deterioration in the hybrid control performance.
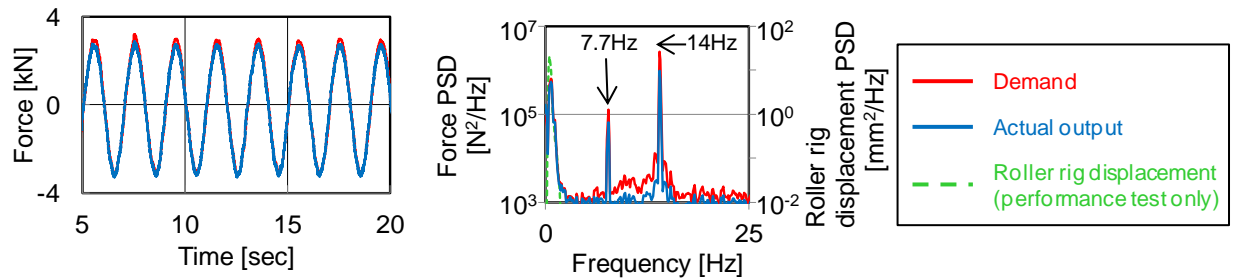
(a) Independent shaking test   (b) Performance test with RSTP

    on test bench

Fig. 4   Comparison of results between independent shaking tests and with RSTP

3. DSS implementation study using an existing test rig

    The objective of this study was to investigate if DSS was a viable framework for the RPB in the following two respects: (1) avoid any deterioration of control performance caused by dynamic coupling and (2) ensure straightforward parameter changeability of the virtual elements. Therefore, the laboratory test system was constructed using an existing rig in Bristol University's Advanced Control and Test Laboratory (ACTLab) and then implemented the corresponding DSS controllers. This section describes the rig and the emulation model, details of DSS controller design and presents the key results from the shaking tests.

3.1 Outline of the new test rig and the emulation model

The ACTLab test rig and its developed schematic form are shown in Fig. 5, and its specifications are listed in Table 1. The rig consists of 2 hydraulic actuators, 2 suspension units, 1 rigid body beam and a dSPACE DSP control system. This rig was chosen as a viable proof-of-concept since it has characteristics that are common to the RPB - in particular, it has multiple actuators attached to the same rigid body component and the existence of rubber bushes to protect RPB actuators from excessive bending moments.
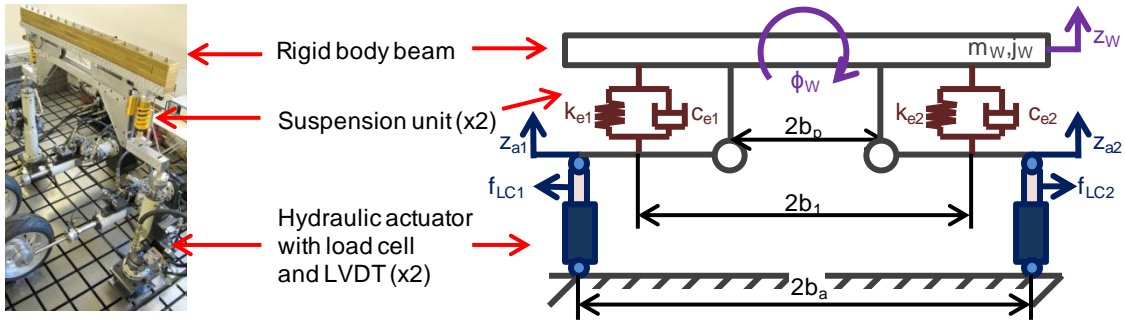
where z_w: vertical displacement of rigid body beam;

ϕ_w: rotational angle of rigid body beam;

z_{a1}, z_{a2}: actuator displacements; and

f_{LC1}, f_{LC2}: external forces from actuators.

Fig. 5   Proof-of-concept test rig

Table 1   Specifications of the rig

Parameter	Description	Value
m_w	Mass of rigid body beam	172 kg
j_w	Moment of inertia about beam	94 kg m^2
k_{e1}, k_{e2}	Suspension spring constants	210 kN/m, 244 kN/m
c_{e1}, c_{e2}	Suspension damping constants	5560 N s/m, 5600 N s/m
$2b_1$	Distance between suspensions	1.3 m
$2b_p$	Distance between pivots of swing-arms	1.1 m
$2b_a$	Distance between actuators	1.7 m

This demonstrator system was a simplification of the actual RPB used by the RSTP. Typically, the RPB is shaken in the lateral direction by roller rigs and a creep force which affects

the wheel-set motion (Fig. 6(b)). Although creep force is a non-linear phenomenon in theory, linear approximations can be applied in the case of small relative motion between wheel and rail. The demonstrator model (Fig. 6(a)) was designed so that it represented a wheel-set supported by 2 primary suspensions and shaken vertically via 2 creep-dampers. The corresponding linearised equations of the model are given by (1) and (2).

In the laboratory test system, each suspension unit was regarded as part of the corresponding hydraulic actuator and each actuator of the rig emulated not only a virtual primary suspension but also virtual creep force.
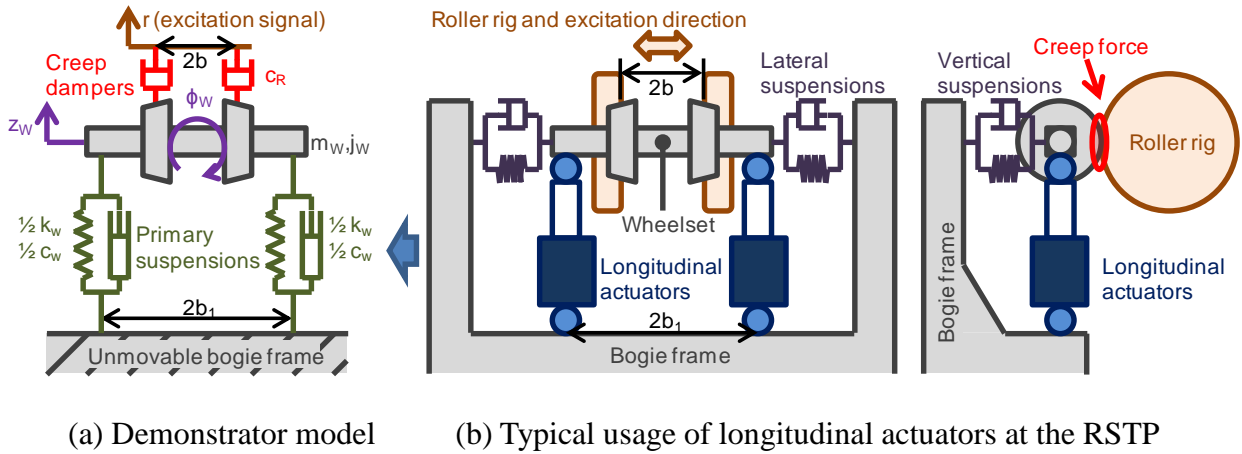

(a) Demonstrator model   (b) Typical usage of longitudinal actuators at the RSTP

Fig. 6   Demonstrator model and typical usage of RPB at the RSTP

$$m_w \ddot{z}_w + c_w \dot{z}_w + k_w z_w = 2c_R(\dot{r} - \dot{z}_w) \tag{1}$$

$$j_w \ddot{\phi}_w + b_1^2 c_w \dot{\phi}_w + b_1^2 k_w \phi_w = -2b^2 c_R \dot{\phi}_w \tag{2}$$

where m_w : mass of wheelset;

j_wJw : moment of inertia about wheelset;

k_w, c_w : stiffness and damping coefficient of primary suspensions; and

c_RCr : damping coefficient of creep-damper.

3. 2 Controller design

In this research, the variables to be synchronised by the DSS controller were the numerical model and actual actuator displacements. This implied that the measured force was treated as an input and the demanded actuator displacement as an output, which was the opposite of the case with the original RPB controller, being introduced for reasons of experimental convenience. Although the original transfer function DSS approach resulted in successful performance using the same ACTLab rig in previous work [5], the state-space DSS approach by the same authors [6] was adopted. It was noted that the synchronising controller of the transfer function based approach is generally of a high order and if applied to the RPB (which is more complex dynamically than the ACTLab rig), numerical conditioning could be a problem.

3.2.1 The state-space DSS approach

Figure 7 shows the framework of the state-space DSS approach based on reference [6]. Here, the entire emulated system is decomposed into two substructures, $\{\Sigma_N, \Sigma_P\}$; Σ_N is the numerical substructure, Σ_P is the physical one. Σ_1 in Σ_N is related to the characteristics of numerically emulated components, Σ_2 in Σ_P to the dynamics of physical test components, and G_{TS} in Σ_P to the transfer system of actuators. In this study, the corresponding dynamic elements are the virtual primary suspensions and creep-dampers, the rigid beam and suspension units, and the hydraulic actuators, respectively. The interaction term between Σ_P and Σ_N, y_i, is a vector of the measured forces f_{LC1} and f_{LC2}. z_P and z_N are the physical and numerical outputs to be synchronised. Actuator displacements are the outputs in this study. Note that in Fig. 7, $\dot{r}$ is used as the reference input, since the transfer function from reference to state variables must be strictly proper in order to formulate the subsequent developments in section 3.2.3. Replacing r by $\dot{r}$ is not a serious problem, since this excitation signal is always known in advance in DSS testing, so that $\dot{r}$ can be determined a priori.
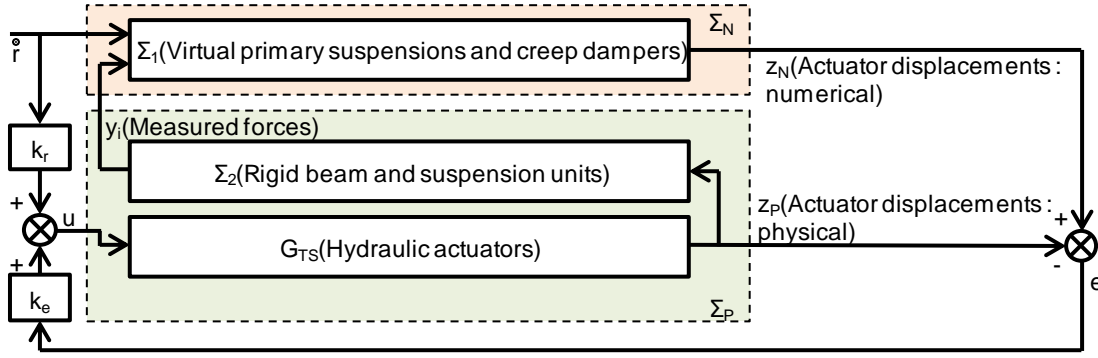
Fig. 7　The DSS framework based on reference [6]

Assuming that state variables of Σ_N and Σ_P contain the synchronizing variables z_N and z_P, respectively, the state and output equations can be written as:

$$\Sigma_N : \begin{pmatrix} \dot{z}_N \\ \dot{z}_{N2} \end{pmatrix} = \begin{pmatrix} A_{N11} & A_{N12} \\ A_{N21} & A_{N22} \end{pmatrix} \begin{pmatrix} z_N \\ z_{N2} \end{pmatrix} + \begin{pmatrix} B_{Ni} \\ B_{Ni2} \end{pmatrix} y_i + \begin{pmatrix} B_{Nr} \\ B_{Nr2} \end{pmatrix} \dot{r} \tag{3}$$

$$z_N = (I \quad 0) \begin{pmatrix} z_N \\ z_{N2} \end{pmatrix} \tag{4}$$

$$\Sigma_P : \begin{pmatrix} \dot{z}_P \\ \dot{z}_{P2} \end{pmatrix} = \begin{pmatrix} A_{P11} & A_{P12} \\ A_{P21} & A_{P22} \end{pmatrix} \begin{pmatrix} z_P \\ z_{P2} \end{pmatrix} + \begin{pmatrix} B_{Pu} \\ B_{Pu2} \end{pmatrix} u \tag{5}$$

$$z_P = (I \quad 0) \begin{pmatrix} z_P \\ z_{P2} \end{pmatrix} \tag{6}$$

$$y_i = (C_{Pi1} \quad C_{Pi2}) \begin{pmatrix} z_P \\ z_{P2} \end{pmatrix} + D_{Pi} u \tag{7}$$

where z_{N2} and z_{P2} are subsets of the state variables of Σ_N and Σ_P, respectively; see (3) ~ (6). Note that all matrices are decomposed into submatrices which have corresponding dimensions of the synchronizing variables and their subsets. From (3) ~ (7), the state equation of the synchronized error $e = z_N - z_P$ is derived as follows:

$$\dot{e} = \dot{z}_N - \dot{z}_P$$

$$= A_{N11}e + (B_{Ni}D_{Pi} - B_{Pu})u$$

$$+A_{N12}z_{N2} + (A_{N11} + B_{Ni}C_{Pi1} - A_{P11})z_P + (B_{Ni}C_{Pi2} - A_{P12})z_{P2} + B_{Nr}\dot{r} \qquad (8)$$

Therefore, assuming that the controllability matrix $[(B_{Ni}D_{Pi} - B_{Pu}) \quad (B_{Ni}D_{Pi} - B_{Pu})A_{N11}]$ is of full rank (e is a 2×1 vector) and that all state variables can be measured, the following control input vector u ensures that $e \to 0$:

$$u = -(B_{Ni}D_{Pi} - B_{Pu})^{-1}A_{N11}e$$

$$-(B_{Ni}D_{Pi} - B_{Pu})^{-1}\{A_{N12}z_{N2} + (A_{N11} + B_{Ni}C_{Pi1} - A_{P11})z_P$$

$$+(B_{Ni}C_{Pi2} - A_{P12})z_{P2} + B_{Nr}\dot{r}\} \qquad (9)$$

The first term on the right-hand side of (9) is the error feedback term $k_e e$ in Fig. 7, and the remainder of the terms constitute the feedforward term $k_r \dot{r}$. In this study, all state variables including z_P can be obtained numerically in order to calculate $k_r \dot{r}$.

3.2.2 Equations of motion and actuator dynamics

In this section, capital letters represent Laplace-transformed variables, e.g. Z_w is the Laplace transformed variable of z_w. Considering that the measured forces F_{LC1} and F_{LC2}, which are obtained from load cells attached in hydraulic actuators (see Fig. 5), are positive in tension, the following is obtained:

$$\begin{pmatrix} F_{LC1} \\ F_{LC2} \end{pmatrix} = -\gamma^2 \begin{pmatrix} g_{e1} & 0 \\ 0 & g_{e2} \end{pmatrix} \begin{pmatrix} Z_{a1} \\ Z_{a2} \end{pmatrix} + \gamma^2 \begin{pmatrix} g_{e1} & b_a g_{e1} \\ g_{e2} & -b_a g_{e2} \end{pmatrix} \begin{pmatrix} Z_w \\ \Phi_w \end{pmatrix} \qquad (10)$$

where g_{e1} and g_{e2} are characteristics of the rig suspension units, and γ is the arm-lever ratio of the suspension unit given by $g_{e1} = c_{e1}s + k_{e1}$, $g_{e2} = c_{e2}s + k_{e2}$, and $\gamma = (b_1 - b_p)/(b_a - b_p)$, respectively. In addition, F_{LC1} and F_{LC2} represent external forces which affect the beam dynamics. In this model, these forces are equal to the outputs of virtual primary suspensions and creep-dampers and are therefore also given by:

$$\begin{pmatrix} Z_w \\ \Phi_w \end{pmatrix} = \begin{pmatrix} \frac{1}{\alpha} & 0 \\ 0 & \frac{1}{\beta} \end{pmatrix} \begin{pmatrix} 1 & 1 \\ b_a & -b_a \end{pmatrix} \begin{pmatrix} F_{LC1} \\ F_{LC2} \end{pmatrix} + \begin{pmatrix} \frac{1}{\alpha} & 0 \\ 0 & \frac{1}{\beta} \end{pmatrix} \begin{pmatrix} 2c_R s \\ 0 \end{pmatrix} R \tag{11}$$

where $\alpha = (2c_R + c_w)s + k_w$, $\beta = (2b^2 c_R + b_1^2 c_w)s + b_1^2 k_w$. From (10) and (11), the relationships for actuator displacements, load cell and excitation signals are determined as follows:

$$\begin{pmatrix} \alpha\beta g_{e1} & 0 \\ 0 & \alpha\beta g_{e2} \end{pmatrix} \begin{pmatrix} Z_{a1} \\ Z_{a2} \end{pmatrix} =$$

$$\begin{pmatrix} \beta g_{e1} + b_a^2 \alpha g_{e1} - \frac{\alpha\beta}{\gamma^2} & \beta g_{e1} - b_a^2 \alpha g_{e1} \\ \beta g_{e2} - b_a^2 \alpha g_{e2} & \beta g_{e2} + b_a^2 \alpha g_{e2} - \frac{\alpha\beta}{\gamma^2} \end{pmatrix} \begin{pmatrix} F_{LC1} \\ F_{LC2} \end{pmatrix} + \begin{pmatrix} 2c_R \beta g_{e1} \\ 2c_R \beta g_{e2} \end{pmatrix} sR \tag{12}$$

Using (10), the equation of the rigid beam motion is derived as follows:

$$\begin{pmatrix} m_w s^2 + \gamma^2 g_{e1} + \gamma^2 g_{e2} & \gamma^2 b_a g_{e1} - \gamma^2 b_a g_{e2} \\ \gamma^2 b_a g_{e1} - \gamma^2 b_a g_{e2} & j_w s^2 + \gamma^2 b_a^2 g_{e1} + \gamma^2 b_a^2 g_{e2} \end{pmatrix} \begin{pmatrix} Z_w \\ \Phi_w \end{pmatrix} = \begin{pmatrix} \gamma^2 g_{e1} & \gamma^2 g_{e2} \\ \gamma^2 b_a g_{e1} & -\gamma^2 b_a g_{e2} \end{pmatrix} \begin{pmatrix} Z_{a1} \\ Z_{a2} \end{pmatrix} \tag{13}$$

Finally, the actuator dynamics are adequately represented by the first-order form ($i = 1, 2$):

$$Z_{ai} = \frac{b_a}{s + a_a} U_i \qquad (14)$$

3.2.3 Derivation of the DSS controller

In (12), which represents the dynamics of Σ_N, the polynomial degrees of Z_{ai}, F_{LCi}, and R are 3, 2 and 3, respectively. This implies that in order to determine a state equation from (12), $\dot{r}$ must replace r in Fig. 7, to ensure strictly proper conditions. With the state vector set to $(z_{Na1}, z_{Na2}, z'_{Na1}, z'_{Na2}, z''_{Na1}, z''_{Na2})^T$, where $z_N = (z_{Na1}, z_{Na2})^T$ and $z_{N2} = (z'_{Na1}, z'_{Na2}, z''_{Na1}, z''_{Na2})^T$, the state equation of Σ_N, corresponding to (3), is given by:

$$
\begin{pmatrix} \dot{z}_{Na1} \\ z_{Na2} \\ z'_{Na1} \\ z'_{Na2} \\ z''_{Na1} \\ z''_{Na2} \end{pmatrix} =
\begin{pmatrix}
a_{11} & 0 & 1 & 0 & 0 & 0 \\
0 & a_{22} & 0 & 1 & 0 & 0 \\
a_{31} & 0 & 0 & 0 & 1 & 0 \\
0 & a_{42} & 0 & 0 & 0 & 1 \\
a_{51} & 0 & 0 & 0 & 0 & 0 \\
0 & a_{62} & 0 & 0 & 0 & 0
\end{pmatrix}
\begin{pmatrix} z_{a1} \\ z_{a2} \\ z'_{a1} \\ z'_{a2} \\ z''_{a1} \\ z''_{a2} \end{pmatrix} +
\begin{pmatrix}
b_{i11} & b_{i12} \\
b_{i21} & b_{i22} \\
b_{i31} & b_{i32} \\
b_{i41} & b_{i42} \\
b_{i51} & b_{i52} \\
b_{i61} & b_{i62}
\end{pmatrix}
\begin{pmatrix} f_{LC1} \\ f_{LC2} \end{pmatrix} +
\begin{pmatrix} b_{N1} \\ b_{N2} \\ b_{N3} \\ b_{N4} \\ b_{N5} \\ b_{N6} \end{pmatrix} \dot{r} \qquad (15)
$$

where a_{mn}, b_{imn}, and b_{Nm} are appropriate coefficients. From (13) and (14), and assuming that the state vector is $(z_{Pa1}, z_{Pa2}, z_w, \phi_w, z'_w, \phi'_w)^T$, where $z_P = (z_{Pa1}, z_{Pa2})^T$ and $z_{P2} = (z_w, \phi_w, z'_w, \phi'_w)^T$, the state equation of Σ_P, corresponding to (5), is given by:

$$
\begin{pmatrix} \dot{z}_{Pa1} \\ z_{Pa2} \\ z_w \\ \phi_w \\ z'_w \\ \phi'_w \end{pmatrix} =
\begin{pmatrix}
-a_a & 0 & 0 & 0 & 0 & 0 \\
0 & -a_a & 0 & 0 & 0 & 0 \\
a_{p31} & a_{p32} & a_{p33} & a_{p34} & 1 & 0 \\
a_{p41} & a_{p42} & a_{p43} & a_{p44} & 0 & 1 \\
a_{p51} & a_{p52} & a_{p53} & a_{p54} & 0 & 0 \\
a_{p61} & a_{p62} & a_{p63} & a_{p64} & 0 & 0
\end{pmatrix}
\begin{pmatrix} z_{Pa1} \\ z_{Pa2} \\ z_w \\ \phi_w \\ z'_w \\ \phi'_w \end{pmatrix} +
\begin{pmatrix}
b_a & 0 \\
0 & b_a \\
0 & 0 \\
0 & 0 \\
0 & 0 \\
0 & 0
\end{pmatrix}
\begin{pmatrix} u_1 \\ u_2 \end{pmatrix} \qquad (16)
$$

where a_{pmn} and b_{pmn} are appropriate coefficients. Finally, from (10) and (16), the interaction term $y_i = (f_{LC1}, f_{LC2})^T$, corresponding to (7), is derived as follows:

$$
y_i = (C_{Pi1} \quad C_{Pi2}) \begin{pmatrix} z_{Pa1} \\ z_{Pa2} \\ z_w \\ \phi_w \\ z'_w \\ \phi'_w \end{pmatrix} + D_{Pi} \begin{pmatrix} u_1 \\ u_2 \end{pmatrix} \tag{17}
$$

Using (15), (16) and (17), all the required state variables can be obtained via numerical simulation and all the sub-matrices required for calculating (9) are directly accessible, so that the feedforward term $k_r \dot{r}$ of the controller can be determined. The feedback gain k_e was evaluated via the MATLAB *place* command, in order to locate the closed-loop pole at $s = -50s^{-1}$.

3.3 Test parameters

There were 3 test conditions, as shown in Table 2: parameters of a virtual primary suspension and the shaking amplitude were varied, as in the case of standard RPB tests (for finding optimal parameters). Track irregularities were chosen to be a random wave of appropriate bandwidth, with a flat velocity spectrum in the frequency from 0.1 to 3Hz, which includes the resonant frequency of the rig.

Table 2   Test conditions

	Case 1	Case 2	Case 3
k_w (kN/m)	400	200	100
c_w (Ns/m)	400	200	100
c_R (Ns/m)		1000	

3.4 Test results

Figures 8 and 9 show the shaking test results of cases 1 and 2, respectively, although case 3 is omitted. In each time history, the observed actuator displacement followed the demand calculated via the numerical model; the corresponding synchronisation error was therefore negligible. Furthermore, in the PSD graphs there were no unexpected peak components, as shown by Fig. 4(b). Therefore, in each case, the performance of the DSS controllers was considered to be very satisfactory.
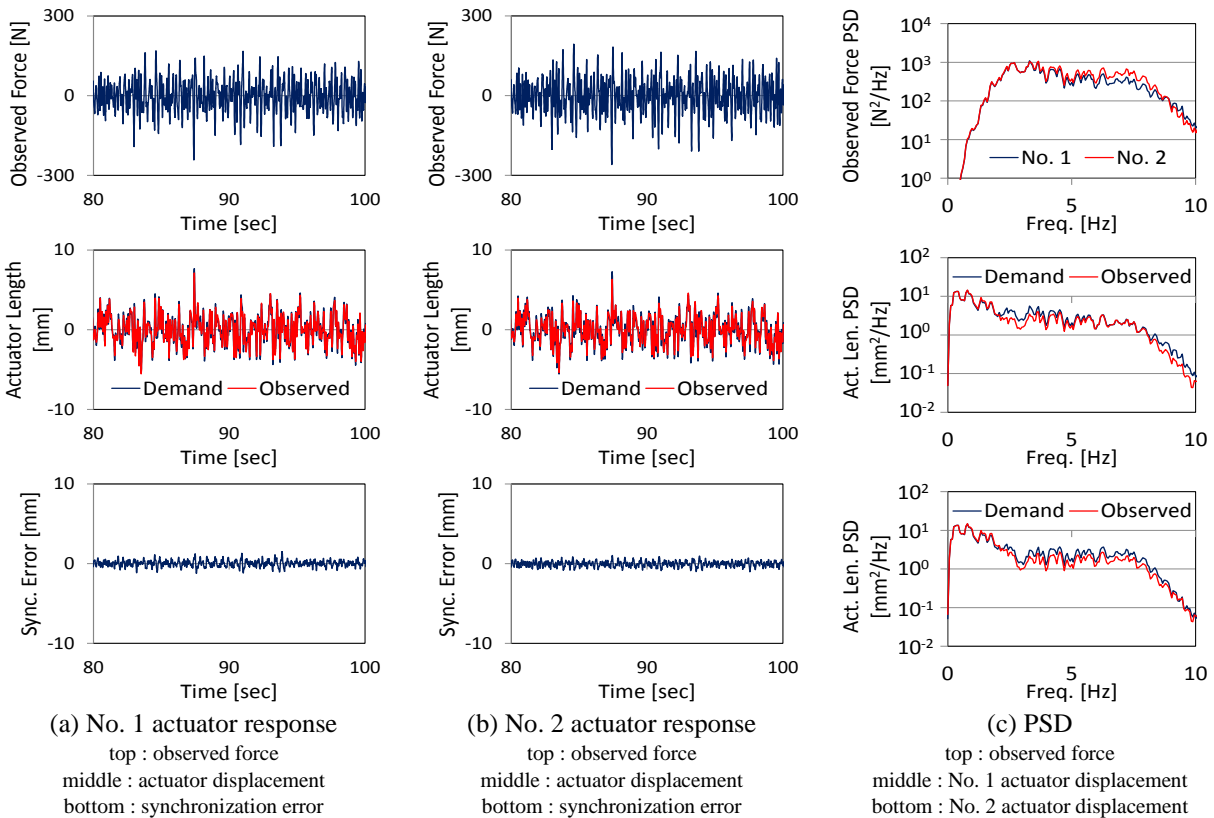

(a) No. 1 actuator response
top : observed force
middle : actuator displacement
bottom : synchronization error

(b) No. 2 actuator response
top : observed force
middle : actuator displacement
bottom : synchronization error

(c) PSD
top : observed force
middle : No. 1 actuator displacement
bottom : No. 2 actuator displacement

Fig. 8   The proof-of-concept rig test results (case 1)

(a) No. 1 actuator response
top : observed force
middle : actuator displacement
bottom : synchronization error

(b) No. 2 actuator response
top : observed force
middle : actuator displacement
bottom : synchronization error

(c) PSD
top : observed force
middle : No. 1 actuator displacement
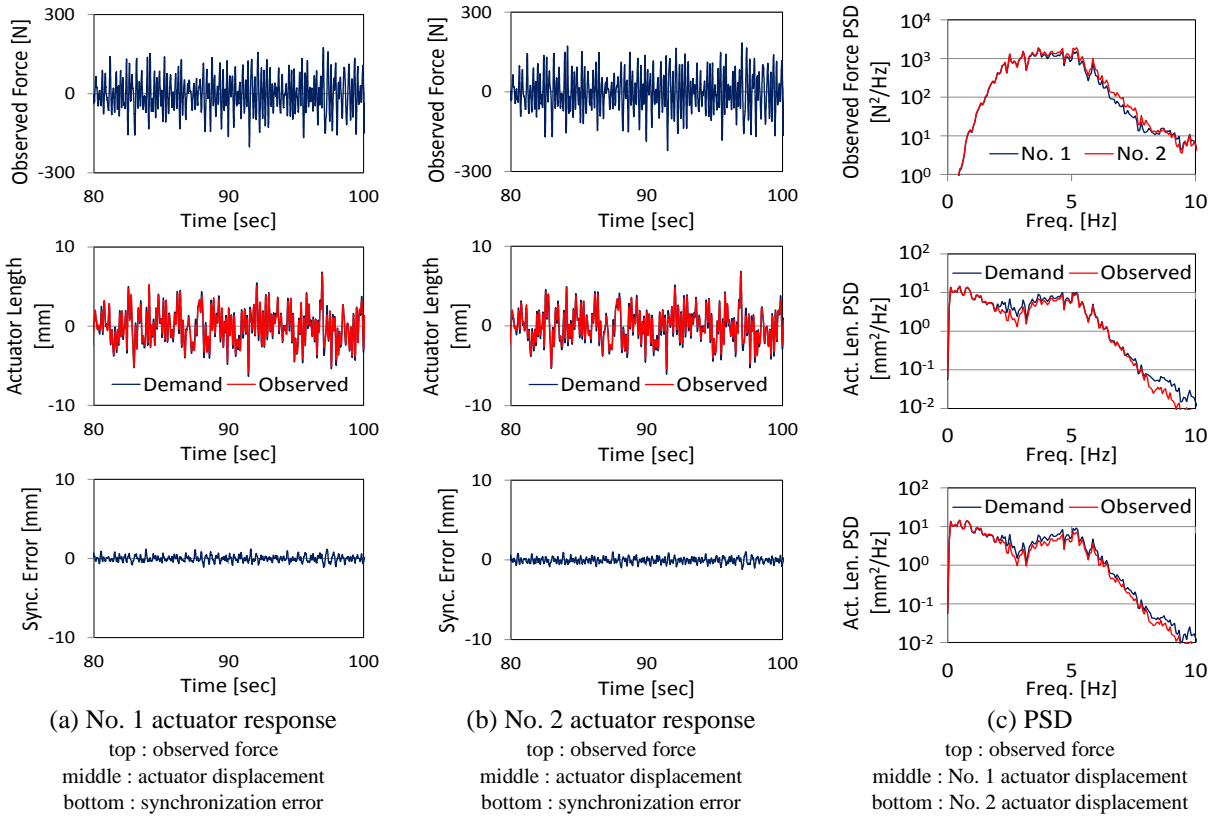bottom : No. 2 actuator displacement

Fig. 9   The proof-of-concept rig test results (case 2)

However, the originally derived feedback gain k_e was found to be too large, with a potential for inducing instability. Therefore reducing its value empirically was found to be necessary. The reason for this was probably due to sensor noise propagation due to the relatively high bandwidth design of the closed-loop pole at s = -50s^{-1}. This suggests the need for a stochastic DSS analysis as an aspect of future work.

4. Discussion

This paper has shown that the proposed DSS controllers were effective in terms of synchronisation between numerical model and actual actuator displacements. This section briefly compares the previous experimental results with simplified simulation results.

Assuming that the characteristics of the rig are perfectly known and that each actuator tracks

its demand perfectly, then $z_{ai} = u_i$. In this case, the rig beam never rotates and its motion will be the same as the motion of the simplified model shown in Fig. 10. In this model, (18), (19) and (20) can be derived; therefore the transfer function from the excitation signal to the actuator displacement is as written in (21). Note that capital letters in (18) ~ (21) represent Laplace-transformed variables shown in Fig. 10.

$$F_{LCi} = -\gamma^2 g_{ei} Z_{ai} + \gamma^2 g_{ei} Z_w \tag{18}$$

$$\frac{1}{2}(m_w s^2 + c_w s + k_w)Z_w = C_R s R \tag{19}$$

$$F_{LCi} = -\frac{1}{2} m_w s^2 Z_w \tag{20}$$

$$\frac{Z_{ai}}{sR} = \frac{C_R}{\gamma^2 g_{ei}} \frac{(m_w s^2 + 2\gamma^2 g_{ei})}{(m_w s^2 + c_w s + k_w)} \tag{21}$$

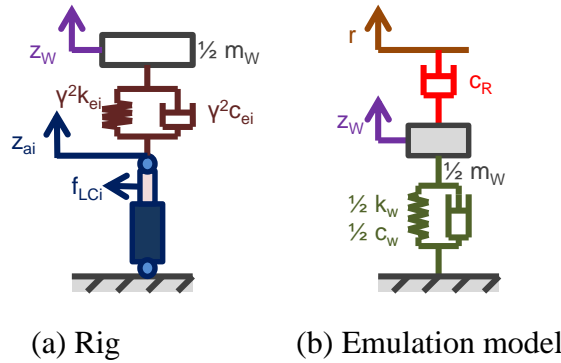(a) Rig   (b) Emulation model

Fig. 10   Simplified rig and emulation model

Figure 11 shows the PSD comparison between the measured actuator displacements and the derived ones from (21). The PSDs are sufficiently close to one another which leads to the conclusion that the designed DSS controllers performed well. However, these tests are effectively restricted to linearisable conditions. One of the most important advantages of DSS testing is the improved understanding of unmodelled phenomena, such as nonlinearity, using actual components. Therefore, testing under more severe conditions will also be the subject of future
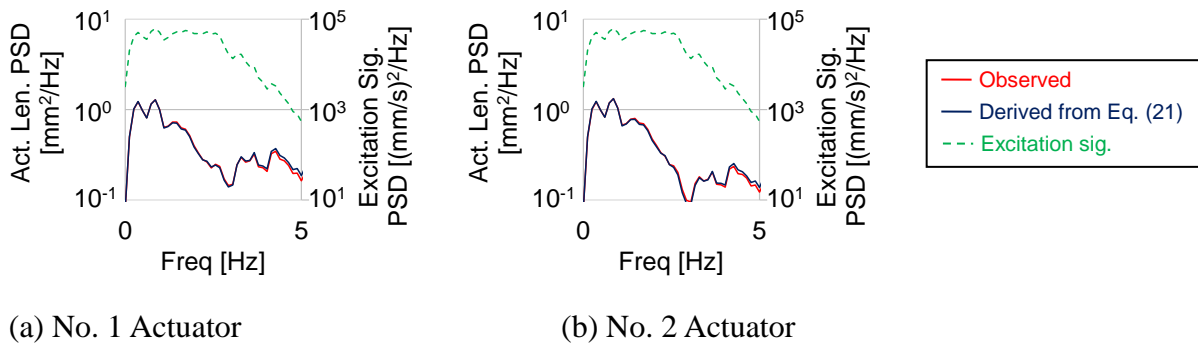
work.

(a) No. 1 Actuator   (b) No. 2 Actuator

Fig. 11   Comparison between experiment and numerical result of case 1

5. Conclusions

In this paper, a DSS strategy to improve the RPB actuator control performance was introduced. The main conclusions are as follows:

A)   A state-space DSS approach was adopted for application to the combination of the existing proof-of-concept rig and a demonstrator model.

B)   Using the rig, shaking tests were conducted and the actuator displacements were well-synchronised with their corresponding numerical models demands. No unexpected motions, which were seen in the original RPB tests at RTRI, were observed.

C)   Application of parameter variations to the tests, using three different virtual suspension parameter sets, resulted in the DSS controllers exhibiting the same degree of excellence in closed-loop performance.

D)   As a consequence, the DSS approach was determined as a viable framework for future research on the RPB system, from the viewpoints of (1) avoidance of the deterioration of control performance caused by dynamic coupling and (2) straightforward parameter changeability of

virtual devices.

References

[1] Watanabe, N. and Stoten, D. P., "Actuator control for a rapid prototyping railway bogie, using a dynamically substructured systems approach," *Proceeding of The 12th International Conference on Motion and Vibration Control (MoViC 2014)*, Paper No. 3D12, 2014.

[2] Morishita, H., Sasaki, K., Shimomura, T. and Watanabe, N., "Development of a Variable Characteristics Test Truck," *Proceedings of J-Rail2010*, pp. 165–168, 2010 (in Japanese).

[3] Watanabe, N., Sasaki, K., Koganei, R. and Morishita, H., "Fundamental Tests on a Rapid Prototype Bogie," *Quarterly Report of RTRI*, Vol. 53, No. 4, pp. 199-204, 2012.

[4] Stoten, D. P. and Hyde, R. A., "Adaptive control of dynamically substructured systems: the single-input single-output case," *Proceedings of the Institution of Mechanical Engineers*, *Part I: Journal of Systems and Control Engineering*, Vol. 220, No. 2, pp. 63-79, 2006.

[5] Stoten, D. P., Tu, J. Y. and Li, G., "Synthesis and control of generalized dynamically substructured systems," *Proceedings of the Institution of Mechanical Engineers*, *Part I: Journal of Systems and Control Engineering*, Vol. 223, No. 3, pp. 371-392, 2009.

[6] Tu, J. Y., Stoten, D. P., Li, G. and Hyde, R. A., "A state-space approach for the control of multivariable dynamically substructured systems," *Proceedings of the Third IEEE Conference on Systems and control*, pp. 1093-1098, 2009.

Authors

Nobuyuki WATANABE
Cheif Researcher, Running Gear Laboratory, Vehicle Structure Technology Division
Research Areas: Vehicle Dynamics, Running Gear Structure

David P. STOTEN, Ph. D.
Professor, Advanced Control & Test Laboratory (ACTLab), Department of Mechanical Engineering, University of Bristol, UK

Research Areas: Dynamic Substructuring, Automatic Control, Servohydraulic System Control